An ultrasound imaging and computational fluid dynamics protocol to assess hemodynamics in iliac vein compression syndrome

Ismael Z. Assi, BSE,[a] Sabrina R. Lynch, PhD,[a] Krystal Samulak, RPhS, RVS,[b] David M. Williams, MD,[c] Thomas W. Wakefield, MD,[b] Andrea T. Obi, MD,[b] *and* C. Alberto Figueroa, PhD,[a,b] *Ann Arbor, MI*

ABSTRACT

Objective: Elevated shear rates are known to play a role in arterial thrombosis; however, shear rates have not been thoroughly investigated in patients with iliac vein compression syndrome (IVCS) owing to imaging limitations and assumptions on the low shear nature of venous flows. This study was undertaken to develop a standardized protocol that quantifies IVCS shear rates and can aid in the diagnosis and treatment of patients with moderate yet symptomatic compression.

Methods: Study patients with and without IVCS had their iliac vein hemodynamics measured via duplex ultrasound (US) at two of the following three vessel locations: infrarenal inferior vena cava (IVC), right common iliac vein, and left common iliac vein, in addition to acquiring data at the right and left external iliac veins. US velocity spectra were multiplied by a weighted cross-sectional area calculated from US and computed tomography (CT) data to create flow waveforms. Flow waveforms were then scaled to enforce conservation of flow across the IVC and common iliac veins. A three-dimensional (3D), patient-specific model of the iliac vein anatomy was constructed from CT and US examination. Flow waveforms and the 3D model were used as a basis to run a computational fluid dynamics (CFD) simulation. Owing to collateral vessel flow and discrepancies between CT and US area measurements, flows in internal iliac veins and cross-sectional areas of the common iliac veins were calibrated iteratively against target common iliac flow. Simulation results on mean velocity were validated against US data at measurement locations. Simulation results were postprocessed to derive spatial and temporal values of quantities such as velocity and shear rate.

Results: Using our modeling protocol, we were able to build CFD models of the iliac veins that matched common iliac flow splits within 2% and measured US velocities within 10%. Proof-of-concept analyses (1 subject, 1 control) have revealed that patients with IVCS may experience elevated shear rates in the compressed left common iliac vein, more typical of the arterial rather than the venous circulation. These results encourage us to extend this protocol to a larger group of patients with IVCS and controls.

Conclusions: We developed a protocol that obtains hemodynamic measurements of the IVC and iliac veins from US, creates patient-specific 3D reconstructions of the venous anatomy using CT and US examinations, and computes shear rates using calibrated CFD methods. Proof-of-concept results have indicated that patients with IVCS may experience elevated shear rates in the compressed left common iliac vein. Larger cohorts are needed to assess the relationship between venous compression and shear rates in patients with IVCS as compared with controls with noncompressed iliac veins. Further studies using this protocol may also give promising insights into whether or not to treat patients with moderate, yet symptomatic compression. (J Vasc Surg Venous Lymphat Disord 2023;11:1023-33.)

Keywords: Iliac vein compression syndrome; May-Thurner syndrome; Computational fluid dynamics; Deep vein thrombosis; Ultrasound Imaging

Iliac vein compression syndrome (IVCS), commonly known as May-Thurner syndrome, is an anatomical variant in which the right common iliac artery compresses the left common iliac vein (LCIV) against the lumbar spine.[1] IVCS is associated with and is thought to play a permissive role in deep vein thrombosis (DVT).[2,3] Despite IVCS anatomy being prevalent in >20% of the population,[1] much remains unclear about the association of IVCS and DVT.

The three broad categories that contribute to DVT pathogenesis, as described by Virchow's triad, are alterations in blood flow, endothelial injury, and hypercoagulability.[4]

From the Department of Biomedical Engineering, University of Michigan[a]; the Section of Vascular Surgery, Department of Surgery,[b] and Division of Interventional Radiology, Department of Radiology,[c] University of Michigan Health System.

This work was funded by the Edward B. Dietrich M.D. professorship in Biomedical Engineering and Vascular Surgery at the University of Michigan. S.L. was supported by the NSF Graduate Research Fellowship Program and the American Heart Association Fellowship (AHA 18PRE33960252). A.O. was supported by the Baiardi Family Foundation.

Author conflict of interest: none.

Additional material for this article may be found online at www.jvsvenous.org.

Correspondence: C. Alberto Figueroa, PhD, Department of Biomedical Engineering, University of Michigan, 2800 Plymouth Rd, Building 20-210W, Ann Arbor, MI 48109 (e-mail: figueroc@med.umich.edu).

The editors and reviewers of this article have no relevant financial relationships to disclose per the Journal policy that requires reviewers to decline review of any manuscript for which they may have a conflict of interest.

2213-333X

https://doi.org/10.1016/j.jvsv.2023.05.017

Venous stasis in upstream veins in the calf and thigh owing to decreased LCIV flow and endothelial damage from arterial pulsations have been proposed as potential mechanisms for the occurrence of DVT in patients with IVCS.[5,6] Furthermore, hypercoagulability is associated with risk factors such as hormonal changes, genetic causes such as Leiden factor V, coronavirus disease 2019, and more.[7,8] One hypercoagulable risk factor that has been overlooked in IVCS is shear activation of platelets, which is often considered as a main contributor to thrombosis initiation in the arterial system.[9] Shear activation of platelets in the arteries typically begins to occur at shear rates of approximately 1000 s^{-1} and is known to contribute to thrombosis initiation by increasing platelet deposition on the vessel wall and platelet-platelet adhesion.[9,10] However, owing to the venous circulation being regarded as a low shear system, the blood shear rate has not been thoroughly investigated thus far as a potential thrombotic mechanism in patients with IVCS.

Venous shear rates are less well-understood than their arterial counterparts, owing to challenges with visualizing the deeper veins using routine imaging and with obtaining reliable and reproducible velocity measurements owing to breathing and vessel motion artifacts. The tool most frequently used to assess venous hemodynamics is ultrasound (US). US scans are highly dependent on the operator and patient body habitus.[11] Furthermore, standard US measures velocity at a given section of the vessel, and assumptions on the venous circulation are made to extrapolate values of flow.[12] Shear rates can then be approximated by dividing the average US velocities by the vessel radius. This approach, however, provides a single value of shear rate for the entire vessel and is, therefore, a significant oversimplification.

One tool that can provide insight on quantities not easily accessible in vivo is computational fluid dynamics (CFD), a well-established technique that uses numerical analysis to solve the equations that describe fluid motion (known as the Navier-Stokes equations). CFD provides high-resolution three-dimensional (3D) hemodynamic descriptions in complex geometries and has been used extensively to assess arterial hemodynamics[13,14] and to assist in surgical planning.[15-17] Hemodynamic quantities computed using CFD, such as velocity, pressure, and shear rate, may explain how fluid dynamics contributes to the biology of venous thrombosis, predict whether patients with moderate but symptomatic compression would benefit from intervention, or in cases of stent failure help to identify the cause of thrombosis.

Challenges in obtaining reliable venous geometry and hemodynamic data, together with the collapsibility of the vessels, have all contributed to the relatively sparse deployment of CFD methods on the venous circulation. Thus, the lack of established venous computational modeling practices motivates the need for a well-designed, controlled research study of venous shear rates in patients with IVCS, which is the purpose of this protocol.

ARTICLE HIGHLIGHTS

- **Type of Research:** Protocol for a single-center, prospective, nonrandomized, case control study
- **Key Findings:** A protocol was developed to measure venous hemodynamics via ultrasound examination, create three-dimensional models of the iliac veins, and compute blood shear rates for a control and a patient with iliac vein compression syndrome (IVCS). Proof-of-concept results suggest that patients with IVCS may experience arterial levels of shear rate.
- **Take Home Message:** This paper presents a proof of concept for a standardized method to study IVCS shear rates using ultrasound examination, computed tomography scans, and computational fluid dynamics.

METHODS

Study design and eligibility criteria

This feasibility study is an off-shoot of a single-center, nonrandomized study conducted at the Diagnostic Vascular Unit at the University of Michigan Medical Center. The study has been approved by the University of Michigan institutional review board (IRB-HUM00212189). Fig 1, *A*, depicts the basic protocol components, which lead to the estimation of blood shear rate in the iliac veins. Fig 1, *B*, summarizes the US data acquisition. The study population consisted of patients aged ≥18 years with IVCS anatomy and DVT and/or lower extremity symptoms (subject group) or with arterial disease and no IVCS anatomy (control group). These patients were selected as controls owing to the readily available computed tomography (CT) data, thereby only requiring venous hemodynamic assessment via US examination. Subjects were recruited as part of an ongoing, actively enrolling trial to evaluate fluid dynamics in the pelvic veins. Patients or controls were excluded from the study if they did not have a recent CT scan on file or if the iliac veins could not be well-visualized with US examination. proof-of-concept results were chosen from this larger patient cohort.

CT scan

An abdominal and pelvic CT scan is performed after intravenous iodinated contrast injection. Because the CT scans in this study were obtained retrospectively, all scans were approved by a board-certified radiologist to ensure that the vessel walls of the iliac veins were well-visualized. Furthermore, given that our methodology for building 3D geometric models of the iliac veins is based on centerline path planning and lofting of contours (see Three-dimensional patient-specific vascular geometries),

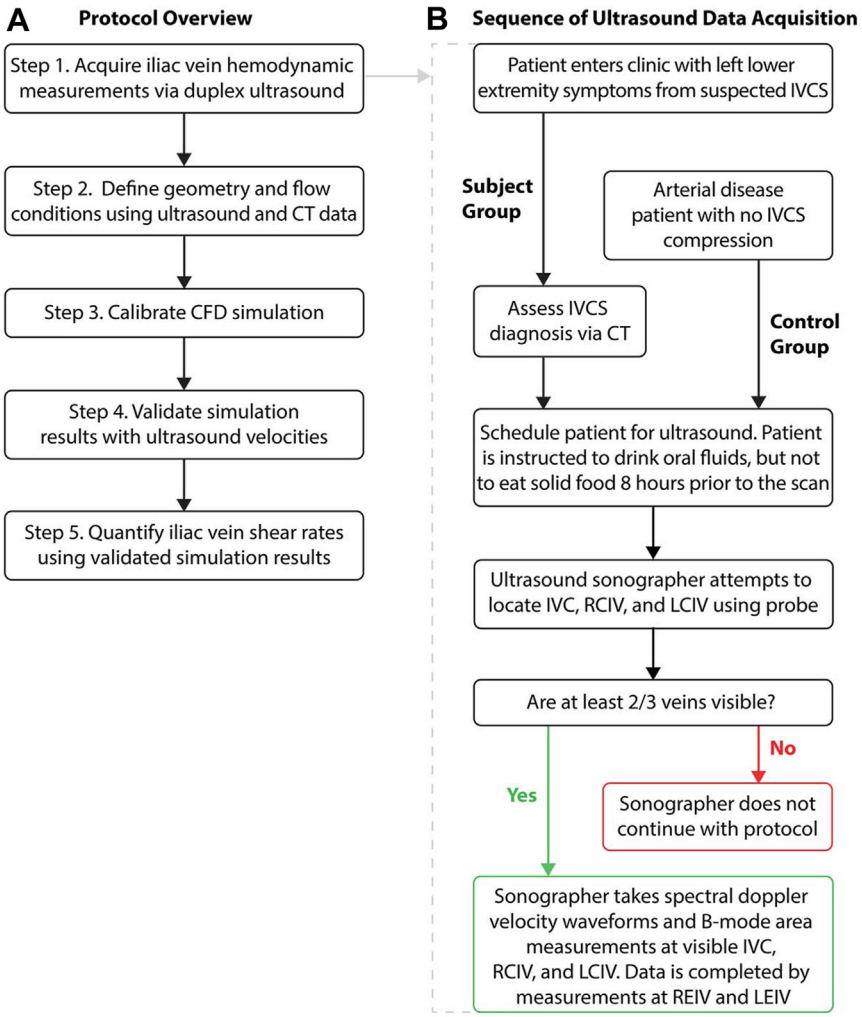

Fig 1. (A) The protocol is outlined by five key steps. **(B)** Once a subject or control has been identified as a study candidate, they are scheduled for an ultrasound (*US*) scan. If the sonographer can visualize at least two of three key locations, velocity and area measurements are acquired via duplex ultrasound (US) examination. *CFD*, Computational fluid dynamics; *CT*, computed tomography; *IVC*, inferior vena cava; *IVCS*, iliac vein compression syndrome; *LCIV*, left common iliac vein; *LEIV*, left external iliac vein; *RCIV*, right common iliac vein; *REIV*, right external iliac vein.

differences in slice thickness between scanners was not considered a significant drawback to our computational models.

US protocol

Patient preparation. Duplex US examination is an imaging technique that is used commonly to evaluate lower extremity veins for deep and superficial venous thrombosis.[18] To improve visualization of the inferior vena cava (IVC) and common iliac veins, patients are instructed to drink fluids, but not to eat solid food for ≥8 hours before the scan. US measurements are taken in the supine position to standardize gravitational effects on areas calculated from US and CT scans. Patients are instructed to breathe normally during US scans. Before the scan, the sonographer measures the patient's respiratory rate. All US imaging in this study is performed with the GE Logiq E9 system and a C1-6 probe. When obtaining spectral Doppler waveforms, the probe's target angle is ≤60° and the pulsed spectral Doppler sample volume is set as the width of the vessel lumen.

Obstruction assessment. To rule out occlusion, venous lower extremity B-mode and spectral Doppler imaging with distal augmentation US scans are performed by taking a dual image with and without compression.[18] Occlusion for the IVC and common iliac veins was evaluated by color and spectral Doppler examination.

Velocity and area assessment. Data acquisition is divided into two parts. First, the sonographer attempts to visualize the infrarenal IVC, right common iliac vein (RCIV), and LCIV. Visualization of two of the three locations is needed to define conservation of flow from the

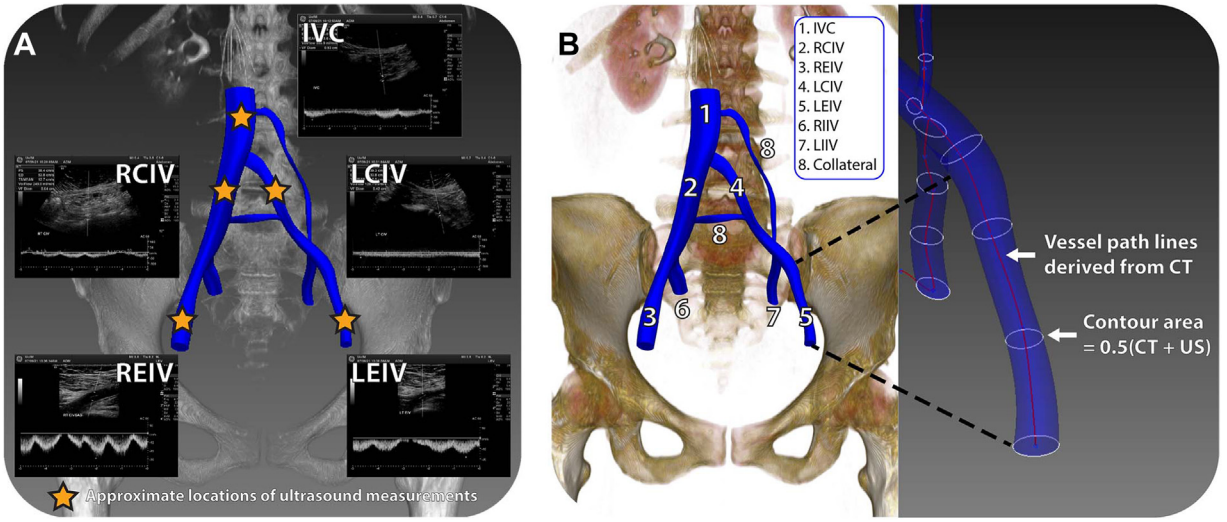

Fig 2. (A) Target locations for ultrasound (*US*) measurements. **(B)** Computed tomography (*CT*) scan-derived path lines and contours. Contour area is adjusted to reflect confidence level in CT and US measurements. The figure shows an example where equal weights were given to the CT and US diameter data. *IVC*, Inferior vena cava; *LCIV*, left common iliac vein; *LEIV*, left external iliac vein; *LIIV*, Left internal iliac vein; *RCIV*, right common iliac vein; *REIV*, right external iliac vein; *RIIV*, right internal iliac vein.

iliac veins into the IVC. If this is not feasible, the patient is excluded. Second, the sonographer begins acquiring velocity and area data. Three different acquisitions are made in each of the visible infrarenal IVC, RCIV, and LCIV. Each acquisition consists of a 5-second spectral Doppler waveform measuring velocity in the sagittal plane and a B-mode image measuring area in the transverse plane. Data are completed by acquiring three different acquisitions of velocity waveforms and area images in each of the right external iliac vein (REIV) and left external iliac vein (LEIV) (Fig 2, *A*). Given that acquisitions are made sufficiently far from a bifurcation or collaterals, the flow through each vessel remains constant, regardless of acquisition location. Therefore, the sonographer was instructed to acquire measurements in the most easily visualized region of each vessel. The three acquisitions of velocity and area also enable assessment of the degree of variability in the data. If variations of >20% are present in either the velocity or cross-sectional area data, further acquisitions are made until consistent measurements are observed.

CFD simulations

Patient-specific computational models are created using the open-source blood flow modeling software CRIMSON.[19] CFD simulations require definition of (i) the 3D geometry of the vessels of interest and (ii) boundary conditions representing the inflow and outflow conditions of the different vessels.

Three-dimensional patient-specific vascular geometries. Geometric models of the iliac veins and IVC are constructed using CT and US data. Because the values of vessel cross-sectional area are known to differ between US and CT measurements,[20,21] we have derived a geometric modeling protocol that enables combining US and CT data to define vessel areas. First, vessel centerlines and contours are created using CT data. The CT-derived vessel contours can then be adjusted further using US data, to reflect the relative level of confidence between the CT and US imaging. Because there are inherent advantages and disadvantages to both CT and US data, geometric models are created with a relative cross-sectional weighting of 50% CT and 50% US data. This weighting is later adjusted during simulation validation. In the example provided by Fig 2, *B*, equal weight was given to CT and US data to define the vessel contour areas.

Inflow and outflow boundary conditions. The US velocity data must be processed to (i) extract flow data, (ii) enforce conservation of flow across the inflow branches and IVC, and (iii) define waveforms over the respiratory cycle. To that end, the following waveform adjustment protocol was developed (Fig 3).

i) Flow waveform extraction: The contours of the 5-second spectral Doppler velocity data for each vessel are digitized using the open-source Plot Digitizer (plotdigitizer.sourceforge.net) software. The contours represent the maximum velocity in the Doppler spectrum. Assuming a parabolic velocity profile, mean velocities can be estimated as 0.5 × maximum velocity. The mean velocities are then multiplied by a weighted average of the US and CT area data to obtain flow waveforms (Fig 3, *A*).

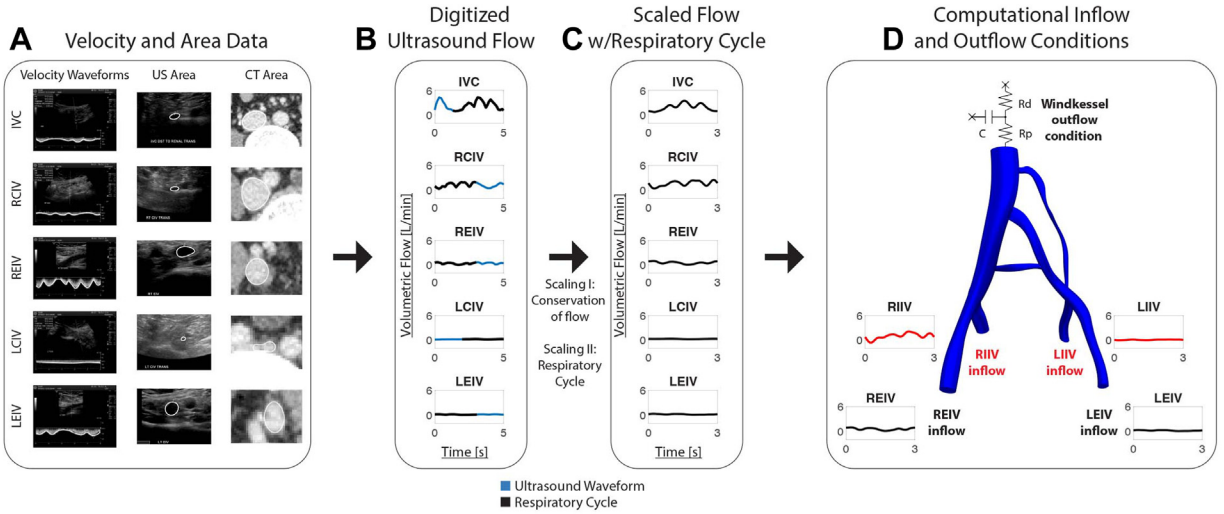

Fig 3. (A) Ultrasound (US) velocity spectra are digitized and then multiplied by a weighted area of the US and computed tomography (*CT*) data to create flow waveforms. **(B)** The flow waveforms are then twice scaled. The first scaling enforces conservation of flow (Supplementary Equations 1-4, online only). **(C)** The second scaling sets a respiratory cycle while maintaining mean flow values. Respiratory cycles are smoothed out using a Fourier interpolation. **(D)** Internal iliac waveforms are estimated through point-by-point subtraction of the external iliac waveforms from the common iliac flow waveforms, then iteratively tuned to account for collateral flow. Measured (right external iliac vein [*REIV*] and left external iliac vein [*LEIV*]) and estimated (right internal iliac vein [*RIIV*] and left internal iliac vein [*LIIV*]) flow waveforms are applied as inflow conditions to the computational model. A Windkessel model is tuned to accommodate the measured inferior vena cava (*IVC*) outflow while setting a mean infrarenal IVC pressure of 10 mm Hg (Supplemental Equations 9-12, online only). *LCIV*, Left common iliac vein; *RCIV*, right common iliac vein.

ii) Conservation of flow across branches: The US flow waveforms are scaled to enforce conservation of flow such that the sum of the inflows is equal to the IVC outflow (Fig 3, *B*) (Supplementary Equations 1-4, online only).
iii) Respiratory cycle scaling: Given that venous flows are influenced greatly by the respiratory cycle,[11,22] the patient's respiratory rate is used to set a periodic cycle on the flow waveforms. The respiratory-adjusted waveforms are scaled such that their mean flows remained unchanged relative to the conservation of flow-adjusted waveforms. Last, the respiratory cycles are smoothed using an 8 mode Fourier interpolation (Fig 3, *C*).

Last, right internal iliac vein (RIIV) and left internal iliac vein (LIIV) waveforms are estimated through point-by-point subtraction of the external iliac waveforms from the common iliac waveforms (Fig 3, *D*). For patients with duplicated internal iliac anatomy, internal iliac waveforms are estimated using the algorithm delineated by Supplementary Equations 5-8 (online only).

REIV, RIIV, LEIV, and LIIV waveforms are then applied as inflow boundary conditions at the model inlets. A three-element Windkessel lumped-parameter model (RCR) consisting of a proximal resistance (R_p), a capacitance (C), and a distal resistance (R_d) is coupled to the infrarenal IVC (Fig 3, *D*). The parameters are tuned so that the average pressure in the infrarenal IVC is 10 mm Hg,[23,24] while accommodating the measured IVC outflow, following an algorithm delineated by Xiao et al[25] (Supplementary Equations 9-12, online only).

The vessel walls are modeled as rigid; therefore, a zero-velocity boundary condition was imposed. Blood is modeled as a non-Newtonian fluid,[26] with viscosity defined by the Carreau-Yasuda model with parameters $\mu_\infty = 0.0035$ Pa·s, $\mu_0 = 0.16$ Pa·s, $n = 0.2128$, $a = 0.64$, and $\lambda = 8.2$ s.[27] Simulations of blood flow and pressure are performed in the Great Lakes high-performance computing cluster at the University of Michigan using 216 cores. The time step size is 0.0001 second. Simulations are run for four respiratory cycles, or until cycle-to-cycle periodicity is observed in the IVC outflow. Mesh independence studies are performed for each patient, with finite element meshes consisting of 2, 4, and 8 million linear tetrahedral elements. Mesh independence was achieved with the 4 million element mesh; therefore, the results reported in this article correspond with that level of mesh refinement.

Flow calibration and velocity validation

Owing to the lack of knowledge on flows through collateral vessels, and the discrepancies between area values between CT and US data, we propose the following adjustment process for flows in internal iliac veins and cross-sectional areas of the common iliac veins (Supplementary Fig 1, online only).

Table. Mean flows (L/min) for subject 1 and control 1

Vessel	Measured	Scaled for conservation	Calibrated simulation	Percentage error
Subject 1				
IVC	2.414	1.917	1.956	
LCIV	0.228	0.308	0.306	0.4
LEIV	0.156	0.211	0.211	
RCIV	1.192	1.609	1.613	−0.2
REIV	0.434	0.586	0.588	
LIIV	NA	0.097	0.195	
RIIV	NA	1.023	0.961	
Ipsilateral collateral	NA	NA	0.036	
Paravertebral collateral	NA	NA	0.063	
Control 1				
IVC	2.200	1.932	1.933	
LCIV	0.597	0.694	0.694	−0.1
LEIV	0.524	0.609	0.609	
RCIV	1.066	1.238	1.239	−0.1
REIV	0.715	0.830	0.831	
LIIV	NA	0.054	0.054	
RIIV	NA	0.408	0.409	
LIIV IIa	NA	0.031	0.031	

Calibrated simulation, calibrated simulated flow; *IVC*, inferior vena cava; *LCIV*, left common iliac vein; *LEIV*, left external iliac vein; *LIIV*, left internal iliac vein; *Measured*, measured flow; *NA*, not applicable; *Percentage error*, percentage error between scaled and calibrated common iliac flow; *RCIV*, right common iliac vein; *REIV*, right external iliac vein; *RIIV*, right internal iliac vein; *Scaled for conservation*, scaling to enforce conservation of flow.

Flow calibration. Discrepancies between simulated and computed common iliac vein flows may be observed. These are caused by flow through collateral vessels that has not been accounted for explicitly in the strategy previously delineated. In that case, internal iliac waveforms are iteratively adjusted until the difference between measured and simulated common iliac vein flows is $<2\%$.

Velocity validation. Because US velocity is the only direct hemodynamic measurement and the key quantity of interest to calculate shear rates, computational results are validated by comparing US velocities against simulated velocities. Simulated velocities are averaged in slices of the RCIV and LCIV. The location of each slice is set to the approximate location of the corresponding US measurement. The mean cross-sectional area of simulated velocities is averaged over the respiratory cycle and then compared with the mean US velocities. If percentage errors of $>10\%$ are observed, the area weighting given to define vessel contour areas using CT and US data is adjusted until a good agreement between simulated and measured velocities is achieved.

RESULTS

As a proof of concept of the modeling technique, we illustrate the proposed protocol with one subject (with IVCS anatomy) and one control (no IVCS anatomy). Subject 1 is a 40-year-old Caucasian female with a body mass index (BMI) of 35. She had a left iliofemoral DVT in 2003 that was treated with thrombolysis. She then re-presented with left femoral-popliteal DVT while she was sick with coronavirus disease pneumonia in 2021. The patient had a history of a factor V Leiden mutation and a family history of DVT, both known risk factors for DVT. The CT scan for subject 1 was acquired using a GE Discovery CT750 HD scanner with a slice thickness of 2.5 mm and venous runoff phase. Control 1 is a 61-year-old Caucasian female with a BMI of 30. She was referred to the US clinic for monitoring of a stenosed carotid artery. The CT scan for control 1 was acquired using a GE LightSpeed VCT scanner with a slice thickness of 1 mm and arterial phase.

Table presents the mean flows for each branch of the vascular models for both patients. Owing to collateral vessel flow in subject 1, adjustments of both LIIV and RIIV flows were required to match LCIV and RCIV flow. Control 1 did not require any flow adjustments.

To define vessel contour areas, equal weighting was given to CT and US cross-sectional area data. Furthermore, to match measured and simulated velocities, cross-sectional area adjustment was required in the LCIV and RCIV for subject 1. No adjustments were required for control 1. The vessel contour area adjustment process for each patient is further detailed in Supplementary Table and Supplementary Fig 2 (online only).

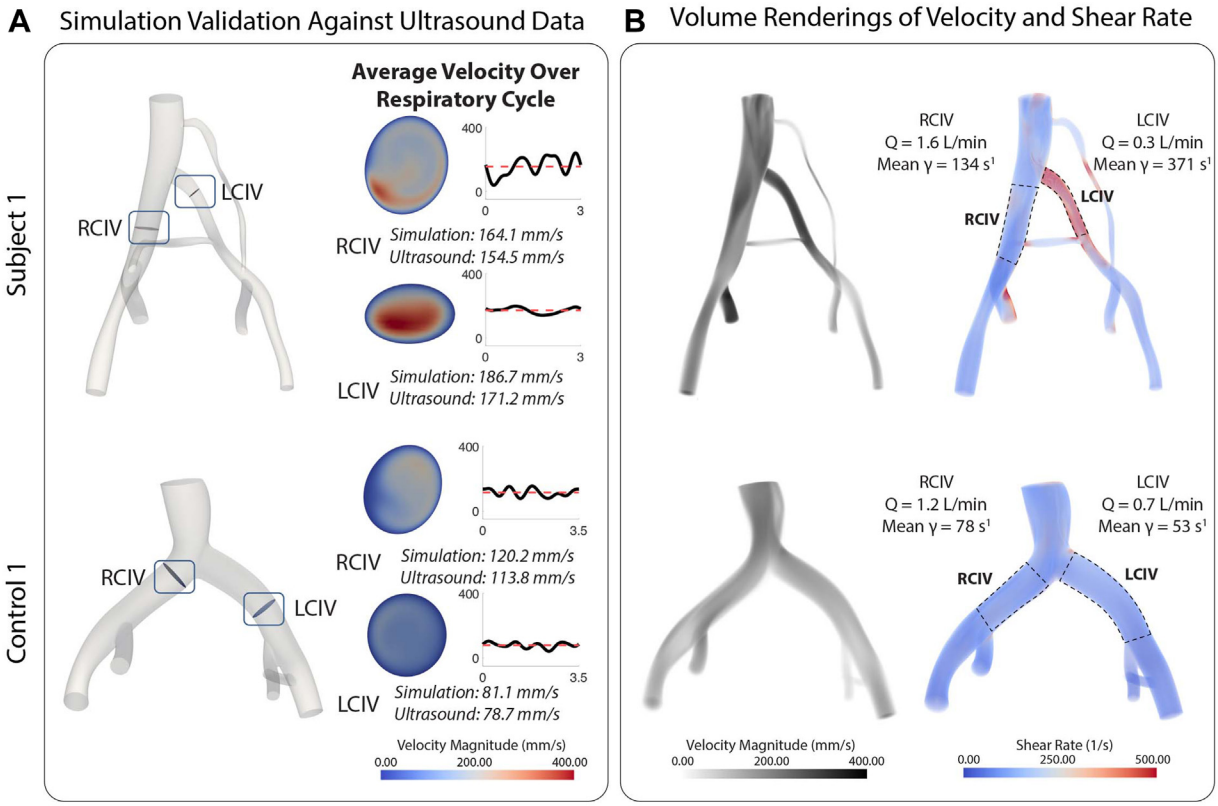

Fig 4. (A) To validate simulation results, slices are taken in the right common iliac vein (*RCIV*) and left common iliac vein (*LCIV*) corresponding with the approximate location of ultrasound (US) measurements. Velocity is averaged in the slices over the respiratory cycle, then compared with the average US velocity. Simulated and measured velocities agreed within 10%. **(B)** Volume renderings of velocity and shear rate are displayed for two patients.

Outflow RCR parameters were tuned to achieve an average IVC pressure of 10 mm Hg. These parameters (mm·g·s base units) are R_p = .0021, C = 27.39, and R_d = 0.0393 for subject 1, and R_p = .0021, C =24.71, and R_d = 0.0394 for control 1.

Fig 4, *A*, displays the validation of simulation velocities with US measurements in slices of the RCIV and LCIV. As stated elsewhere in this article, the adjustment method outlined in Supplemental Fig 1 (online only), discrepancies between simulated and measured velocities are <10%. Fig 4, *B*, displays representative volume renderings of velocity magnitude (mm/s) and shear rate (s^{-1}) for both patients. To further illustrate the effect of venous compression on subject 1's iliac vein hemodynamics, Supplementary Fig 3 (online only) displays subject 1's volume renderings of velocity and shear supplanted with anatomical renderings of their iliac arteries and pelvic bones. The shear rate $\dot{\gamma}$ was calculated as the double contraction of the rate of deformation tensor.[26] Fig 5 displays the shear rate average and interquartile range over the respiratory cycle for both patients. Subject 1 displayed elevated shear rates in the LCIV, with shear rate Q1, mean, and Q3 of 220 s^{-1}, 371 s^{-1}, and 495 s^{-1}, respectively. Furthermore, subject 1 displayed larger shear rates in the compressed region of the LCIV, with shear rate Q1, mean, and Q3 of 298 s^{-1}, 511 s^{-1}, and 705 s^{-1}, respectively. The shear rate ratios for the LCIV/RCIV and compressed LCIV/RCIV were 3.4 and 4.7, respectively. Control 1 did not display elevated shear rates in the LCIV, with shear rate Q1, mean, and Q3 of 18 s^{-1}, 53 s^{-1}, and 82 s^{-1}, respectively. The mean shear rate ratio for LCIV/RCIV was 0.7.

DISCUSSION

The accepted treatment for thrombotic patients with IVCS is to lyse or extract clot, which might be present and stent the underlying iliac vein stenosis.[28] For patients with nonthrombotic IVCS, there is significant variability in clinical management, especially for mild symptoms of venous insufficiency. Physicians have had no tool by which to quantify, categorize, and monitor pelvic vein inflow in patients who have been or are about to be treated with stents. Some physicians treat conservatively with compression stockings and/or anticoagulant therapies, whereas others treat aggressively by stenting the compressed or atretic vein.[29] Differences

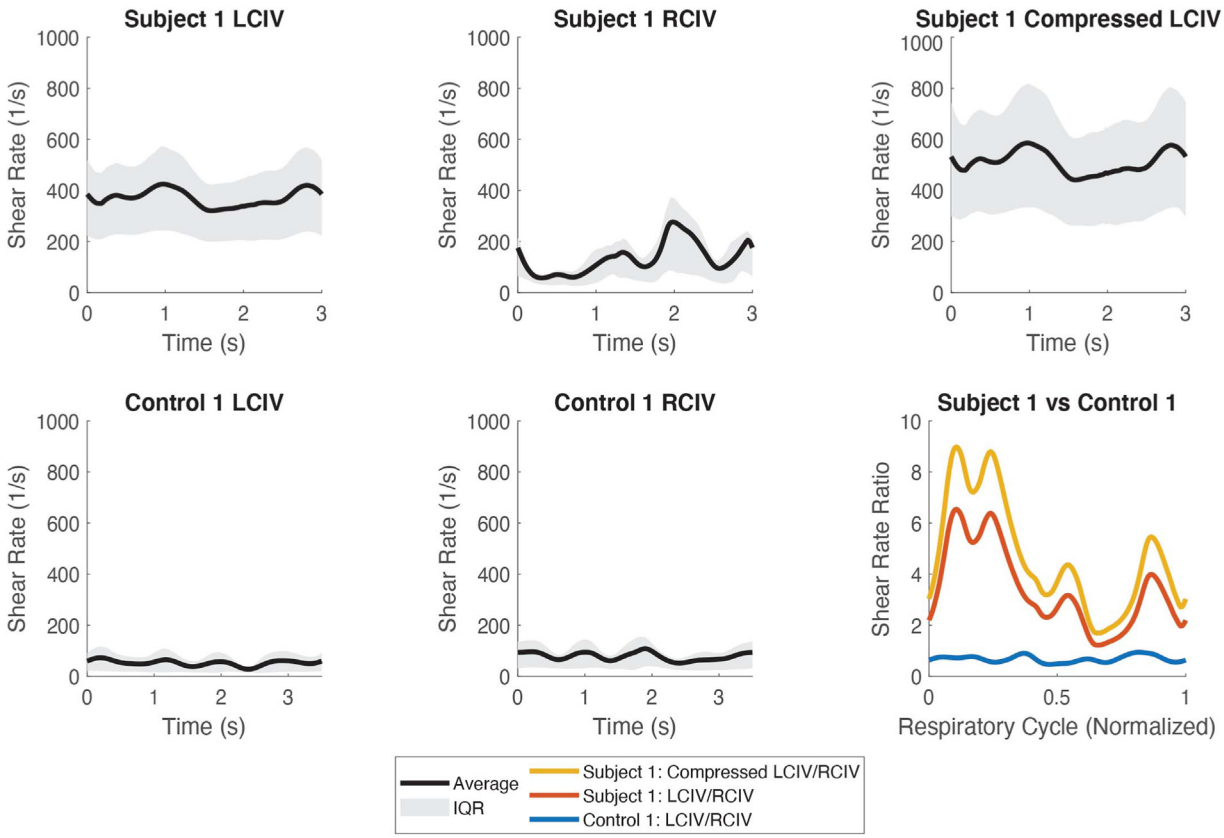

Fig 5. Plots of shear rate over the respiratory cycle. The shear rate average, interquartile range, and ratios are plotted in representative volumes for subject 1 and control 1. Subject 1 displayed elevated left common iliac vein (*LCIV*) shear rates, especially in the compressed region, whereas control 1 did not display elevated LCIV shear rates. *RCIV,* Right common iliac vein.

in interpretation of the available imaging and hemodynamic data may lead to differences in treatment approaches.

In those patients with moderate yet symptomatic compression, our CFD models give a high-resolution description of both global and local hemodynamics, which can help elucidate the mechanics or instigating factors of thrombus formation. Results reported here revealed that patients with IVCS may experience elevated shear rates, which are more typical of the arterial circulation than the venous circulation. Better understanding the mechanics of thrombus formation will further help in developing iliac vein hemodynamic characterization tools with clinically relevant timelines.

The proposed CFD method could also provide insights into which patients would benefit from stenting vs conservative treatment or help to detect obstruction after venous intervention at earlier states. Another instance in which this method can provide further insights relative to simple evaluation of US waveforms is in cases of patients with robust collaterals, where normal upstream waveforms cannot exclude obstructions in the iliocaval confluence. The proposed protocol, by combining CT and US imaging with CFD, provides characterization of flow and shear rates through the axial veins and larger collaterals, including proximal and obstructed segments.

As a single-center, nonrandomized, case control study, the generalizability of these results may be limited. Larger patient cohorts from multiple centers must be evaluated to establish whether elevated shear rates could be a potential contributing mechanism for thrombosis initiation in patients with IVCS. These analyses should also be performed in varying positions (supine, reverse Trendelenburg, standing, etc) so that the effects of gravity on iliac vein hemodynamics can be evaluated, especially in patients who are symptomatic only when standing or walking.

During US imaging, visualizing the IVC and common iliac veins during US imaging may be challenging owing to vessel motion during breathing, bowel gas, and body habitus. These challenges were addressed by instructing the patient to breathe normally and not to eat solid foods before the scan. We found that deep inspiration or expiration caused the IVC and common iliac veins to move, making US acquisitions difficult. Instructing the

patient to breathe normally circumvented this issue. Future work could examine the effects of deep inspiration and expiration on venous hemodynamics via intravascular US (IVUS) examinations. Furthermore, instructing the patient not to consume solid foods for ≥8 hours before the scan decreases the amount of bowel gas, improving visualization of the IVC, RCIV, and LCIV greatly. However, hydration status is important for blood volume and may affect hemodynamics as measured via US.[11] Thus, to ensure that US measurements are representative, we recommend instructing the patient to drink fluids as usual before the US scan. Despite the improved visualization from not consuming solid food, the depth of the IVC, RCIV, and LCIV can potentially make data acquisition difficult. To decrease scan times, US data acquisition is split into a location phase and an acquisition phase.

While postprocessing US and CT data, US area measurements were observed to differ from CT area measurements sometimes by over 100%. These discrepancies are due to several reasons, such as the US and CT scans not being performed on the same day and the impact of the patient's hydration status on vessel cross-sectional area.[11] The time interval between CT and US scans was 4 and 1 weeks for subject 1 and control 1, respectively.

Depending on the level of confidence in the data, area weighting can be adjusted in the model to favor CT or US measurements. Furthermore, velocity and area measurements can vary within the same scan, depending on the pressure applied by the sonographer and the angle of interrogation used to visualize veins. To verify that velocity and area measurements are precise, we recommend taking at least three images of each measurement at each location.

The exclusion criteria for patients whose iliac veins cannot be well-visualized via US examination favors a lower BMI; increased body habitus makes visualization of the IVC and common iliac veins via duplex US examination more difficult. In the results presented, both patients had a BMI of >30. Obtaining velocity and area measurements via phase-contrast magnetic resonance imaging (MRI) or IVUS may be superior to duplex US examination in patients with larger body habitus. Phase contrast MRI or IVUS would also circumvent the need for assuming a parabolic velocity profile for the Doppler US waveforms, which may not hold true in the iliac veins owing to blood's non-Newtonian viscosity, vessel stiffness, and the noncircular nature of iliac vein cross-sectional areas. However, phase contrast MRI is more costly and IVUS examination presents limitations, such as its invasiveness and imaging artifacts from shadowing and air bubbles.[30]

Furthermore, because shear rate is the gradient of blood velocity, that is, the change in velocity divided by the change in radius, errors in measuring velocity or area will directly impact the resulting shear rate calculation. In this work, we strived for an accurate matching of the measured velocity (Fig 4, *A*), but uncertainties in the area remain.

Shear rate is also sensitive to physiological factors affecting either velocity or luminal area, such as cardiac output, pressure-volume conditions, blood viscosity, smooth muscle tone, collateral engagement, and other factors. Constraining a patient's hydration status or alternative flow estimation techniques, such as surface integration of velocity vectors,[12] may further standardize measurement of shear rates. The remaining variables are difficult to standardize, and it is likely that shear rates measured 1 day may not be consistent with shear rates measured 2 weeks later. However, because the RCIV can act as matched pair to normalize iliac vein hemodynamics, the ratio of LCIV to RCIV shear rate is a promising metric to standardize the characterization of iliac vein hemodynamics. Further studies are needed to investigate whether the LCIV/RCIV shear rate ratio is correlated with the incidence of DVT, lower extremity venous symptoms, or stent patency.

Our computational models are run under rigid wall assumptions; however, veins can have large variations in cross-sectional area during the respiratory cycle. Variations in LCIV cross-sectional area are small owing to its compression by the right common iliac artery and the lumbar spine.[6] Therefore, our simulations should reasonably estimate LCIV shear rate. However, our analysis may overestimate RCIV shear rates owing to vessel expansion during peak flow (not accounted for by our model), which decreases the velocity gradient and, therefore, the shear rate. This factor could lead to an underestimation of the LCIV/RCIV shear rate ratio and is a limitation to the present study. Future work could examine the effects of vessel wall motion on venous hemodynamics in the iliac veins.

The principle of flow conservation at the iliocaval confluence, which was used to make US flow waveforms suitable for computational analysis, may not apply in patients with severe iliac vein narrowing or occlusion. Collateral flow from obstructed veins in the pelvis drain through the ascending lumbar veins into the azygos system, through the left ovarian vein to the left renal vein, or through the superior hemorrhoidal vein to the portal vein, thus bypassing the iliocaval confluence altogether. Our exclusion criteria for patients whose iliac veins cannot be well-visualized via CT scan tends to exclude those patients with severe LCIV obstruction. Because patients with severe compression are evident on CT scans and can be treated directly, our fluid dynamics models are more suited to investigate whether or not to treat patients with symptomatic, but less severe, compression.

Owing to patient-specific differences in venous anatomy, factors such as arterial flow distribution to each leg, recruitment of collaterals, presence of competing

pathways, and variable vessel lengths or luminal area can lead to bilateral differences in flow through the common or external iliac veins. For example, control 1 demonstrated a mean RCIV flow 1.8 times that of their LCIV (Table). A larger RCIV volumetric flow increased RCIV shear rate and, thus, decreased the measured LCIV/RCIV shear rate ratio.

Contributing to patient-specific differences in venous anatomy is that patients with uncomplicated IVCS will likely have a lower resistance than that of IVCS complicated by iliofemoral DVT (owing to the length of the vessel stenosis and rigid walls resulting from inflammatory responses). Therefore, given the same decrease in lumen size, patients with uncomplicated IVCS will be expected to have a larger mean LCIV volumetric flow, and correspondingly a larger shear rate. The larger shear rates, however, will only be observed over a shorter segment of the vessel as compared with a patient with IVCS complicated by iliofemoral DVT. From this standpoint, given the history of left iliofemoral venous thrombosis, subject 1 may not be an optimal choice to represent nonthrombotic patients with IVCS.

Furthermore, because subject 1's LCIV has a high resistance owing to the underlying IVCS and chronic DVT inflammatory responses, flow through their upstream vessels such as the external and internal iliac veins was likely diverted through alternative pathways. For example, the measured REIV flow for subject 1 was >2.5 times than that of the LEIV (Table). Given the increased LCIV resistance, subject 1's estimated LIIV flow is larger than expected and is similar to presumedly normal flow for healthy patient (Table). However, part of this flow is directed through the two collaterals in the anatomical model (and even other collateral not accounted for in the model). As stated in the Methods, RIIV and LIIV flows were not directly measured from US examination, but instead estimated by subtracting external iliac waveforms from common iliac waveforms, enforcing conservation of flow through the system.

Patients with IVCS may also undergo cycles of thrombus formation and resolution.[31] Therefore, the timing of each scan in the DVT formation-resolution cycle will impact observed hemodynamics. A growing thrombus in the LCIV in the presence of collateral veins may lead to different situations regarding LCIV shear rate. For instance, even though a thrombus in the LCIV decreases the effective lumen size, the velocity (and therefore the shear rate) may not necessarily increase relative to its prethrombotic value, because a portion of the flow may be diverted through collateral veins owing to the increase in LCIV resistance from the thrombus. In the results presented, both patients were imaged with no thrombus present.

Last, the protocol outlined in this article is time consuming, not only because of the time it takes for the simulations to run, but also because of the time it takes to process the image data and make them suitable for analysis. This factor severely affects the clinical applicability of the proposed workflow. To address this limitation and based on our proof-of-concept findings, our team has developed an US-based monitoring tool that estimates shear rates quickly (on the order of seconds). We are currently performing a prospective study in which shear rates estimated using the US-based monitoring tool are validated using the protocol outlined in this article. The prospective study will include a larger patient cohort, with varying types of obstruction. The US-based monitoring tool will also be used before and after thrombotic events to investigate hemodynamic changes owing to post-thrombotic responses and to assess whether the tool can predict clinical outcomes, such as stent patency and risk of thrombus formation.

CONCLUSIONS

In this protocol, we presented a standardized method to measure venous hemodynamics, create patient-specific computational models of the iliac veins, and compute blood shear rates, which are promising in symptomatic patients with moderate narrowing. Proof-of-concept analyses have revealed that patients with IVCS may experience shear rates more typical of the arterial system. More investigation is needed to assess the relationship between venous compression, shear rate, and DVT and/or lower extremity venous symptoms.

Computational resources were provided by NSF Grant-1531752 and Advanced Research Computing at the University of Michigan, Ann Arbor, Michigan.

AUTHOR CONTRIBUTIONS

Conception and design: IA, SL, KS, DW, AO, CAF
Analysis and interpretation: IA, SL, DW, TW, AO, CAF
Data collection: IA, KS, AO
Writing the article: IA, CAF
Critical revision of the article: IA, SL, KS, DW, TW, AO, CAF
Final approval of the article: IA, SL, KS, DW, TW, AO, CAF
Statistical analysis: IA
Obtained funding: AO, CAF
Overall responsibility: IA

REFERENCES

1. May R, Thurner J. The cause of the predominantly sinistral occurrence of thrombosis of the pelvic veins. Angiology 1957;8:419-27.
2. Thijs W, Rabe KF, Rosendaal FR, Middeldorp S. Predominance of left-sided deep vein thrombosis and body weight. J Thromb Haemost 2010;8:2083-4.
3. Raju S, Neglen P. High prevalence of nonthrombotic iliac vein lesions in chronic venous disease: a permissive role in pathogenicity. J Vasc Surg 2006;44:136-44.
4. Brotman DJ, Deitcher SR, Lip GYH, Matzdorff AC. Virchow's triad revisited. South Med J 2004;97:213-4.
5. Kaltenmeier CT, Erben Y, Indes J, et al. Systematic review of May-Thurner syndrome with emphasis on gender differences. J Vasc Surg Venous Lymphat Disord 2018;6:399-407.e4.
6. Zucker EJ, Ganguli S, Ghoshhajra BB, Gupta R, Prabhakar AM. Imaging of venous compression syndromes. Cardiovasc Diagn Ther 2016;6:519-32.

7. Rosendaal FR. Venous thrombosis: a multicausal disease. Lancet (London, England) 1999;353:1167-73.
8. Mehta JL, Calcaterra G, Bassareo PP. COVID-19, thromboembolic risk, and Virchow's triad: lesson from the past. Clin Cardiol 2020;43:1362-7.
9. Sakariassen KS, Orning L, Turitto VT. The impact of blood shear rate on arterial thrombus formation. Futur Sci OA 2015;1:FSO30.
10. Ruggeri ZM. The role of von Willebrand factor in thrombus formation. Thromb Res 2007;120:1-10.
11. Meissner MH, Moneta G, Burnand K, et al. The hemodynamics and diagnosis of venous disease. J Vasc Surg 2007;46:4-24.
12. Kripfgans OD, Rubin JM, Hall AL, Gordon MB, Fowlkes JB. Measurement of volumetric flow. J Ultrasound Med 2006;25:1305-11.
13. Figueroa CA, Taylor CA, Marsden AL. Blood flow. In: Stein E, de Borst R, Hughes TJR, editors. Encyclopedia of computational mechanics. Second. John Wiley & Sons; 2017.
14. Taylor CA, Figueroa CA. Patient-specific modeling of cardiovascular mechanics. Annu Rev Biomed Eng 2009;11:109-34.
15. Ahmed Y, Tossas-Betancourt C, van Bakel PAJ, et al. Interventional planning for endovascular revision of a lateral tunnel Fontan: a patient-specific computational analysis. Front Physiol 2021;12:1-11.
16. Van Bakel TM, Arthurs CJ, Van Herwaarden JA, et al. A computational analysis of different endograft designs for Zone 0 aortic arch repair. Eur J Cardiothoracic Surg 2018;54:389-96.
17. van Bakel TMJ, Lau KD, Hirsch-Romano J, Trimarchi S, Dorfman AL, Figueroa CA. Patient-specific modeling of hemodynamics: supporting surgical planning in a Fontan circulation correction. J Cardiovasc Transl Res 2018;11:145-55.
18. Youn YJ, Lee J. Chronic venous insufficiency and varicose veins of the lower extremities. Korean J Intern Med 2019;34:269-83.
19. Arthurs CJ, Khlebnikov R, Melville A, et al. CRIMSON: an open-source software framework for cardiovascular integrated modelling and simulation. PLoS Comput Biol 2021;17:e1008881.
20. Han SM, Patel K, Rowe VL, Perese S, Bond A, Weaver FA. Ultrasound-determined diameter measurements are more accurate than axial computed tomography after endovascular aortic aneurysm repair. J Vasc Surg 2010;51:1381-9.
21. Jaakkola P, Hippelainen M, Farin P, Rytkonen H, Kainulainen S, Partanen K. Interobserver variability in measuring the dimensions of the abdominal aorta: comparison of ultrasound and computed tomography. Eur J Vasc Endovasc Surg 1996;12:230-7.
22. Moneta GL, Bedford G, Beach K, Strandness DE. Duplex ultrasound assessment of venous diameters, peak velocities, and flow patterns. J Vasc Surg 1988;8:286-91.
23. Laborda A, Sierre S, Malvè M, et al. Influence of breathing movements and Valsalva maneuver on vena caval dynamics. World J Radiol 2014;6:833-9.
24. Tedaldi E, Montanari C, Aycock KI, Sturla F, Redaelli A, Manning KB. An experimental and computational study of the inferior vena cava hemodynamics under respiratory-induced collapse of the infrarenal IVC. Med Eng Phys 2018;54:44-55.
25. Xiao N, Alastruey J, Figueroa CA. A systematic comparison between 1-D and 3-D hemodynamics in compliant arterial models. Int J Numer Method Biomed Eng 2014;30:204-31.
26. Lynch S, Nama N, Figueroa CA. Effects of non-Newtonian viscosity on arterial and venous flow and transport. Sci Rep 2022;12:20568.
27. Abraham F, Behr M, Heinkenschloss M. Shape optimization in steady blood flow: a numerical study of non-Newtonian effects. Comput Methods Biomech Biomed Engin 2005;8:127-37.
28. Peters M, Syed RK, Katz M, et al. May-Thurner syndrome: a not so uncommon cause of a common condition. SAVE Proc 2012;25:231-3.
29. Hng JZK, Su S, Atkinson N. May—Thurner syndrome, a diagnosis to consider in young males with no risk factors: a case report and review of the literature. J Med Case Rep 2021;15:1-7.
30. McLafferty RB. The role of intravascular ultrasound in venous thromboembolism. Semin Intervent Radiol 2012;29:10-5.
31. Meissner MH, Caps MT, Bergelin RO, Manzo RA, Strandness DEJ. Propagation, rethrombosis and new thrombus formation after acute deep venous thrombosis. J Vasc Surg 1995;22:558-67.

Submitted Jan 28, 2023; accepted May 17, 2023.

Additional material for this article may be found online at www.jvsvenous.org.

APPENDIX (online only).

Scaling to enforce conservation of flow across branches. US flow waveforms are scaled to enforce conservation of flow such that the sum of the iliac vein inflows is equal to the IVC outflow. Here, two scenarios are possible.

1. If all three flow measurements are available, namely, $Q_{IVC}^{measured}$, $Q_{RCIV}^{measured}$, and $Q_{LCIV}^{measured}$, the measured IVC flow will generally not match the sum of RCIV and LCIV flows. Therefore, the following corrections are made. We first define a calculated IVC flow as:

$$Q_{IVC}^{calculated} = Q_{RCIV}^{measured} + Q_{LCIV}^{measured}. \quad (1)$$

Next, a corrected IVC flow is defined as:

$$Q_{IVC}^{corrected} = \frac{Q_{IVC}^{calculated} + Q_{IVC}^{measured}}{2}. \quad (2)$$

This correction represents a weighted average of the direct IVC flow measurement, and that given by the sum of RCIV and LCIV measurements. The following scaling factor for IVC flow is defined as:

$$k_{IVC}^{scaling} = \frac{Q_{IVC}^{corrected}}{Q_{IVC}^{measured}}. \quad (3)$$

Finally, a scaling factor for the RCIV and LCIV flows is defined as:

$$k_{branches}^{scaling} = \frac{Q_{IVC}^{corrected}}{Q_{IVC}^{calculated}}. \quad (4)$$

This scaling factor is also applied to the REIV and LEIV flow measurements.

2. If the sonographer was not able to visualize the IVC, RCIV, or LCIV, the missing vessel's flow is estimated by enforcing: $Q_{IVC} = Q_{RCIV} + Q_{LCIV}$.

Estimating flow waveforms for a duplicated internal iliac vein. A duplicated internal iliac vein is a normal variation within iliac venous anatomy. If a patient presents with a duplicated internal iliac, flow splits through the main branch and duplicated branch are calculated as follows. First, we estimate an internal iliac waveform (IIV) through point-by-point subtraction of the external iliac waveform (EIV) from the common iliac waveform (CIV):

$$IIV = CIV - EIV. \quad (5)$$

Next, we calculate a flow split ratio (β) based on the cross-sectional area of the main branch (A_{main}) and the duplicated branch ($A_{duplicated}$). This scaling ratio assumes that the two branches behave as parallel resistors and that their resistance can be approximated by Poiseuille's law:

$$\beta = \frac{A_{main}^2}{A_{main}^2 + A_{duplicated}^2}. \quad (6)$$

Last, to estimate the internal iliac main branch (IIV_{main}) and duplicated branch ($IIV_{duplicated}$) flow waveforms, the flow split ratio is applied to the internal iliac waveform (IIV):

$$IIV_{main} = \beta * IIV \quad (7)$$

$$IIV_{duplicated} = (1 - \beta) * IIV. \quad (8)$$

Tuning the infrarenal IVC Windkessel lumped-parameter model. A Windkessel lumped-parameter model consisting of R_p, C, and R_d is coupled to the infrarenal IVC. The sum of proximal and R_d is the total IVC resistance (R_T). The parameters are tuned such that the average pressure in the infrarenal IVC is 10 mm Hg while accommodating the measured IVC outflow, following an algorithm delineated by Xiao 2014[25] (Equations 9-12).

$$R_T = \frac{\text{Pressure}}{Flow} = \frac{10\ mmHg}{Flow_{IVC}} \quad (9)$$

$$R_p = 0.05 * R_T \quad (10)$$

$$R_d = 0.95 * R_T \quad (11)$$

$$C = \frac{(Flow_{IVC,MAX} - Flow_{IVC,MIN}) * \Delta t_{MAX-MIN}}{2 * 10\ mmHg} \quad (12)$$

Supplementary Table (online only). Mean cross-sectional areas (mm^2) for subject 1 and control 1

Vessel	CT	US	Target	Validated
Subject 1				
IVC	316	97	207	207
LCIV	32	15	23	29
LEIV	64	42	53	53
RCIV	222	43	132	172
REIV	147	36	92	92
LIIV	50	NA	34	34
RIIV	113	NA	78	78
Ipsilateral collateral	13	NA	9	9
Paravertebral collateral	18	NA	12	12
Control 1				
IVC	322	196	259	259
LCIV	141	112	126	126
LEIV	131	155	143	143
RCIV	190	141	165	165
REIV	120	140	130	130
LIIV	40	NA	38	38
RIIV	81	NA	77	77
LIIV IIa	30	NA	28	28

CT, Measured computed tomography area; *IVC*, inferior vena cava; *LCIV*, left common iliac vein; *LEIV*, left external iliac vein; *LIIV*, left internal iliac vein; *RCIV*, right common iliac vein; *REIV*, right external iliac vein; *RIIV*, right internal iliac vein; *Target*, target area reflecting equal weighting given to CT and ultrasound data; *US*, measured ultrasound area; *US*, ultrasound; *Validated*, area adjusted to match measured and simulated velocities.

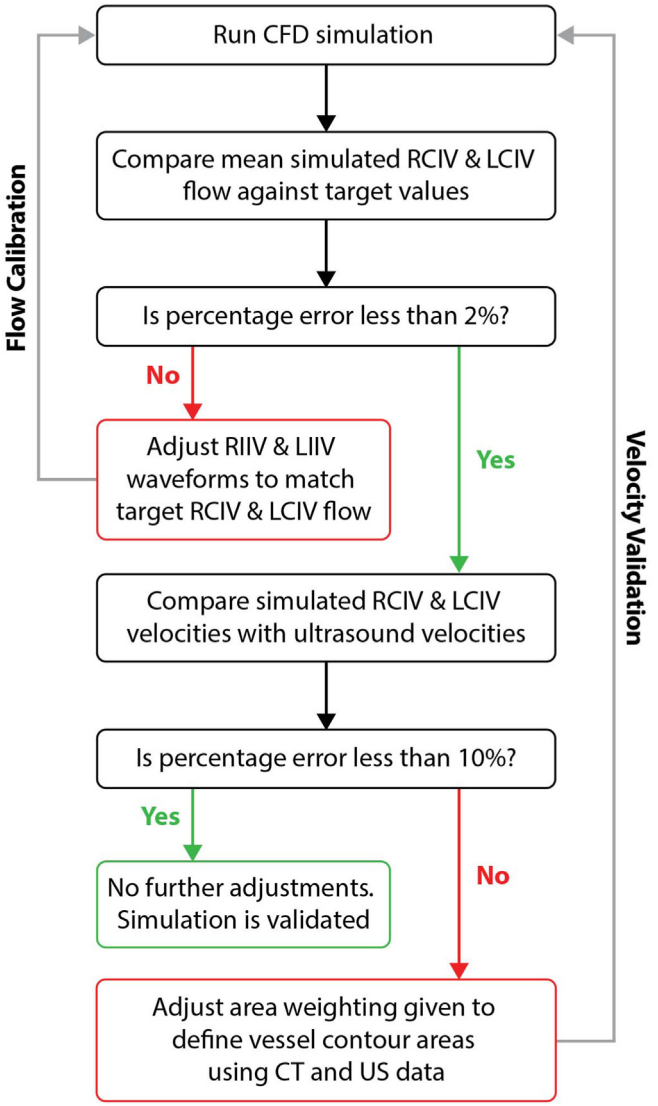

Supplementary Fig 1 (online only). Adjustment process for internal iliac flow and cross-sectional areas of the common iliac veins. This strategy accounts for flow through collateral vessels and the discrepancies between area values in computed tomography (*CT*) and ultrasound (*US*) data. *CFD*, computational fluid dynamics; *LCIV*, left common iliac vein; *LIIV*, left internal iliac vein; *RCIV*, right common iliac vein; *RIIV*, right internal iliac vein.

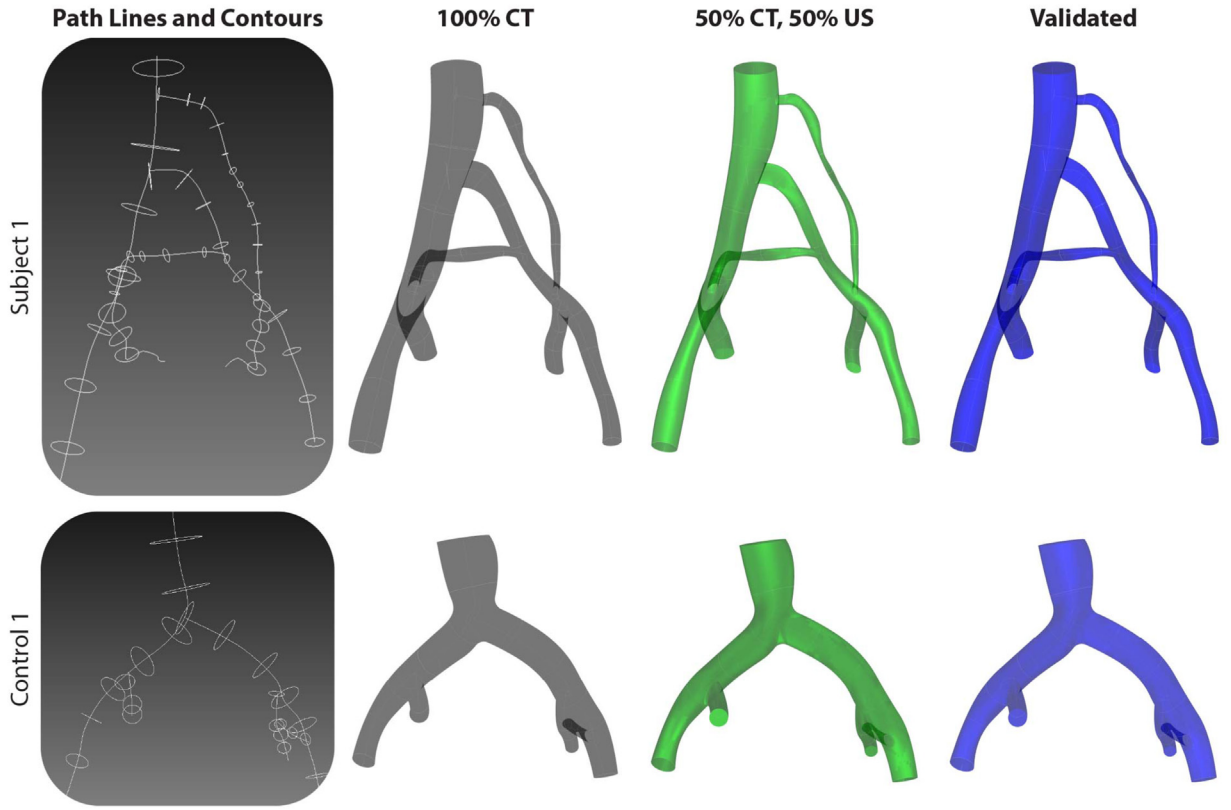

Supplementary Fig 2 (online only). Contour area adjustment process. Computed tomography (*CT*)-derived path lines and contours, 3D vascular model with 100% CT area weighting, 3D vascular model with 50% CT and 50% ultrasound (*US*) area weighting, and the validated model are displayed for each patient.

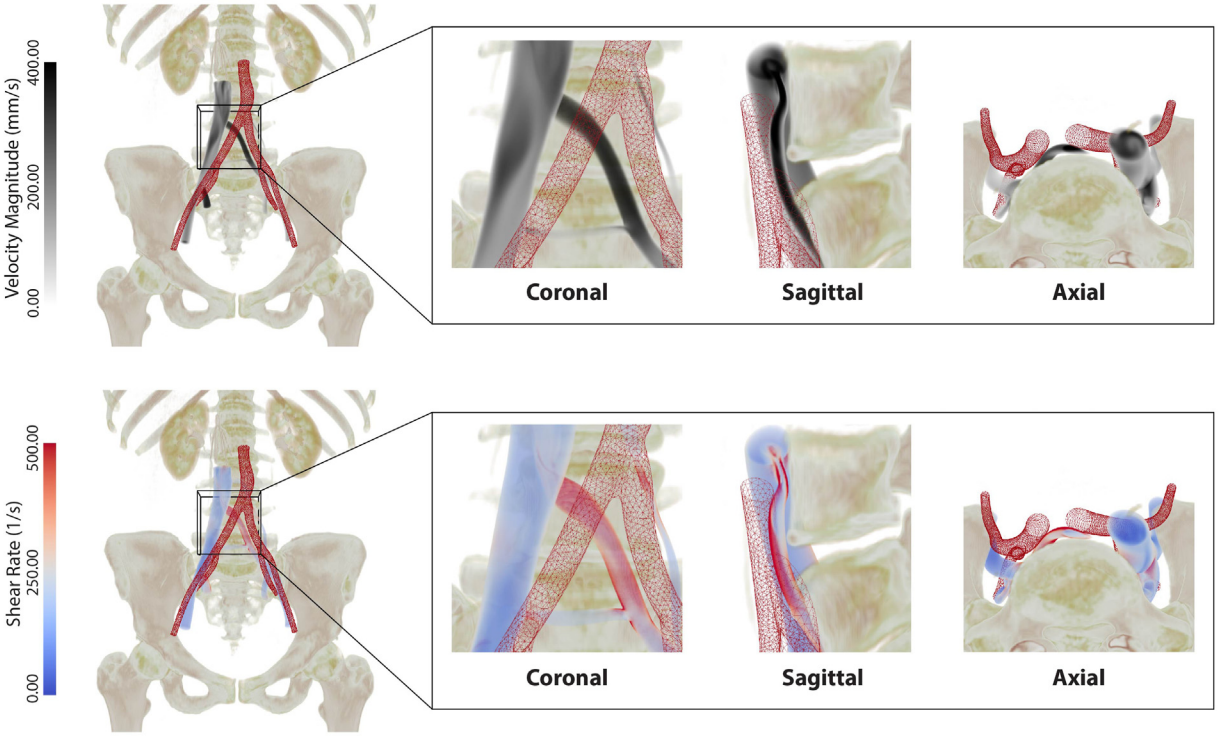

Supplementary Fig 3 (online only). To further illustrate the effect of venous compression on subject 1's iliac vein hemodynamics, their simulation volume renderings of velocity and shear rate at peak left common iliac vein (LCIV) flow are supplanted with anatomical renderings of subject 1's iliac arteries and pelvic bones. The figure also contains magnified views from coronal, sagittal, and axial perspectives.